# Alectinib Polypharmacology Enhances Response to Spliceosome Disruption

**Authors:** Yurui Ma[1], Evon Poon[2], Chenchen Jin[1], Barbara Martins da Costa[2], Yuewei Xu[1,3], Sadiya Quazi[1], Nikolaos Zourdoumis[1], Chiharu Wickremesinghe[1], Louis Chesler[2], Hector C Keun[1]*, Anke Nijhuis[1]*¥

**Affiliations:**

[1]Department of Surgery & Cancer, Imperial College London; London, UK.

[2]Division of Clinical Studies, The Institute of Cancer Research, London, UK

[3]Wisdom Lake Academy of Pharmacy, Xi'an Jiaotong-Liverpool University, Suzhou 215123, China (current affiliation)

**Running title:** Synergistic RNA Splicing Disruption via SRPK1 and RBM39

***Co-corresponding author**

¥**Lead contact:** Dr Anke Nijhuis

**Address**: Division of Cancer, Imperial College London, London, UK, W12 0NN.

**Email**: a.nijhuis@imperial.ac.uk **Phone**: +44 (0) 20 7594 3161

**Conflict of interest disclosure statement:** Authors declare that they have no conflict of interest.

**Other notes:** 5233 words; 7 figures; 7 supplementary figures; 1 supplementary table

**Abstract:** RNA splicing is essential for gene expression regulation and is frequently dysregulated in cancer. A degrader of RNA splicing factor RBM39, indisulam, can induce aberrant splicing and shows potent anti-cancer activity, creating vulnerabilities that can be exploited by combinatorial approaches. Through combinatorial drug-screening, we identified a synergistic interaction between indisulam and alectinib, a clinical ALK inhibitor that also inhibits serine/arginine protein kinase 1 (SRPK1), a key splicing regulator. Co-treatment with indisulam and alectinib inhibited cell proliferation, induced apoptosis, and caused G2–M arrest in multiple cancer cell lines, including *MYCN*-amplified neuroblastoma. RNA sequencing revealed enhanced splicing defects preferentially in DNA damage response related genes following combination treatment, leading to R-loop accumulation and increased DNA damage. In the Th-MYCN/ALK$^{F1174L}$ neuroblastoma mouse model, combination therapy induced complete tumour regression and significantly improved survival rates compared with monotherapies. This strategy highlights the therapeutic potential of co-targeting functionally interdependent RNA splicing factors in aggressive cancers.

**Significance:** Our work demonstrates that combining indisulam and alectinib is a promising approach to treat aggressive malignancies such as high-risk neuroblastoma, exploiting the previously untapped polypharmacology of alectinib as a clinical RNA splicing inhibitor and supporting the concept that co-targeting interdependent splicing factors can yield highly synergistic therapies for hard-to-treat cancers.

## INTRODUCTION

The splicing of precursor messenger RNAs (pre-mRNAs) is a critical regulatory step in gene expression, during which non-coding introns are excised to produce functional mRNA(1). This process is tightly controlled by splicing factors, governing the recognition and selection of splice sites, thereby generating mRNAs with varying exon combinations and consequently diverse protein isoforms(1). Dysregulated alternative splicing can promote tumorigenesis and chemoresistance. Aryl sulfonamides such as indisulam have emerged as promising anticancer agents by targeting a RNA splicing factor RBM39 (RNA binding motif 39)(2, 3). These molecular glues facilitate the association of RBM39 with the CUL4-DCAF15 ubiquitin ligase, resulting in RBM39 polyubiquitination and subsequent proteasomal degradation(2, 4). Suppressing RBM39 efficiently inhibits tumour growth and advancement through modulating the transcription of various genes associated with tumorigenesis (reviewed in (3)).

One cancer type particularly vulnerable to splicing perturbation is neuroblastoma(5), a common and aggressive extracranial solid tumour in young children, and a major contributor to paediatric cancer mortality(6). High-risk neuroblastoma, comprising approximately 15% of all neuroblastoma cases, represents a distinct subtype characterized by aggressive tumour behaviour and an unfavourable prognosis(7). One pivotal factor contributing to the progression of high-risk neuroblastoma is the amplification of the MYC family transcription factor, MYCN, which can block the differentiation of neural progenitors, the key event in neuroblastoma initiation(8), and plays a crucial role in facilitating the transcriptional repression of tumour suppressor genes(6, 7). Furthermore, oncogenic gain-of-function mutations in the *ALK* (Anaplastic Lymphoma Kinase) occur in 10–15% of primary tumours, making ALK the most common single-gene alteration in high-risk neuroblastoma for which targeted clinical therapies have been developed(6, 9) Alectinib,

60 an FDA-approved ATP-competitive ALK tyrosine kinase inhibitor (TKI),was initially developed
61 for non-small-cell lung cancer and has shown considerable promise in addressing neuroblastoma
62 in extensive preclinical studies(10-12). However, tumour heterogeneity and resistance to treatment
63 with ALK inhibitors (and molecularly-targeted drugs in general) limit their efficacy as
64 monotherapies(13). Thus, novel strategies, particularly combination therapies, remain important
65 as a means to reduce the toxicity of any single drug and overcome treatment resistance more
66 efficiently. This approach is particularly advantageous in childhood cancer, where long-term
67 toxicity is a major lifelong issue (14).
68
69 Our previous study(15) and others(16) have recognized the exquisite sensitivity of high-risk
70 neuroblastoma to indisulam, with complete responses observed in multiple xenografts, patient-
71 derived xenografts (PDX) and transgenic mouse models. Notably, our study reported that cells
72 with MYCN amplification displayed heightened sensitivity to aryl sulfonamides in comparison to
73 those without MYCN amplification. This could be attributed to the increased reliance of
74 neuroblastoma cells on RNA processing due to elevated N-Myc/c-Myc activity, rendering them
75 more susceptible to RNA splicing interference (17). Through the induction of splicing errors in
76 genes within key oncogenic pathways, indisulam can render cancer cells susceptible to additional
77 disruptions caused by other anticancer drugs. For example, we previously showed that several
78 DNA damage repair (DDR) genes—including *BRCA1, RAD51D*, and *ATM*—are mis-spliced
79 following RBM39 depletion, increasing sensitivity to PARP inhibitors in ovarian high-grade
80 serous carcinoma(18).
81

82 In this study, we aimed to identify additional vulnerabilities through drug-drug library screens
83 combining indisulam with FDA approved anti-cancer agents across various cancer models,
84 including colorectal (HCT116), ovarian (Kuramochi). Through this, we demonstrate a novel
85 synergistic interaction between indisulam and ALK-inhibitor alectinib, likely due to activity
86 against a recently discovered secondary target of alectinib, RNA Serine-Arginine Protein Kinase
87 1 (SRPK1) (19). SRPK1 promotes the nuclear translocation and activation of a family of SR
88 splicing factors (SRSFs). The combination of indisulam and alectinib simultaneously depletes
89 RBM39 and inhibits SRPK1-mediated SRSF phosphorylation, resulting in exacerbated RNA
90 splicing defects. The subsequent failure to resolve accumulated DNA damage and R loops results
91 in cell cycle arrest, cell growth inhibition and apoptosis of neuroblastoma cells *in-vitro* and tumour
92 regression *in vivo*. Our study provides important proof-of-concept evidence for the co-targeting of
93 splicing factors as a viable strategy to treat aggressive malignancies such as MYCN-driven high-
94 risk neuroblastoma.

95

96 **RESULTS**

97 **Combination drug screens revealed synergy between indisulam and alectinib.**

98 We previously demonstrated that indisulam-mediated RBM39 degradation causes wide-spread
99 RNA splicing defects, and an enrichment in aberrant expression of proteins that mediate DNA
100 damage repair and cell cycle regulation, across various cancer types(15, 18, 20). This led us to
101 speculate that indisulam is likely to generate drug-induced-vulnerabilities that potentiate the
102 efficacy of existing, clinically approved anti-cancer compounds, such as PARP inhibitors(18).
103 RBM39 degraders, such as indisulam and E7820, have been trialed in 47 clinical studies(3),
104 highlighting potential therapeutic combinations ready for clinical evaluation.

105

106 To explore this concept, we conducted two drug-library screens combining indisulam with 147
107 FDA-approved anticancer drugs (NCI plate number #4891, #4892) in an indisulam-sensitive cell
108 line (HCT116, colorectal cancer) and an indisulam-resistant line (KURAMOCHI, ovarian cancer).
109 Drugs were tested at 5 doses (16 nM to 10 μM) and combined with DMSO or indisulam at fixed
110 doses (GI30=50 nM for HCT116, 10 μM for KURAMOCHI) (**Fig. 1A, Fig. S1A**). Bliss scores(21)
111 were calculated to identify synergistic interactions with indisulam. Depletion of RBM39 by
112 indisulam is dependent on DCAF15 expression, thus we generated CRISPR-Cas9 knockouts of
113 *DCAF15* to identify RBM39-specific drug-drug interactions (HCT116 *DCAF15* wild-type
114 (*DCAF15*$^{WT}$) clone #1 and #2 and *DCAF15* knock-out clones (*DCAF15*$^{KO}$) clone #1 and #2).
115 Drugs with Bliss score>0 in both HCT116-*DCAF15*$^{WT}$ clones were selected as hits which were
116 further validated in triplicate experiments with selected doses in both HCT116-*DCAF15*$^{WT}$ and
117 *DCAF15*$^{KO}$ clones #1 and #2 and ranked by mean Bliss scores of both cell lines. Most of the
118 synergistic drug-drug interactions were rescued in HCT116-*DCAF15*$^{KO}$ cells suggesting that the
119 synergy is dependent on *DCAF15* and RBM39 degradation (**Fig. 1B left**). In KURAMOCHI, the
120 top 20 hits were ranked by mean Bliss scores across all doses (**Fig. 1B right**). The clinical ALK
121 inhibitor alectinib demonstrated strong synergy in both HCT116 (top hit) and KURAMOCHI
122 (second hit) and was therefore selected for further validation using a wider range of drug
123 concentrations. Strong synergistic growth inhibition was observed across a range of doses of
124 indisulam and alectinib in HCT116 (**Fig. 1C**) and KURAMOCHI (**Fig. 1D**), and the synergy was
125 abrogated in HCT116-*DCAF15*$^{KO}$ cells.

126

127 These data confirm that combining alectinib with RBM39 degraders yields synergistic growth
128 inhibition, supporting a potential combination therapy across diverse cancer types.
129
130 **Indisulam and alectinib exhibit synergistic anticancer efficacy in high-risk neuroblastoma**
131 Considering the potency demonstrated by both indisulam and alectinib as monotherapies in high-
132 risk neuroblastoma(11, 15), we further investigated the combination of indisulam and alectinib in
133 four high-risk neuroblastoma cell lines (KELLY, IMR32, SKNBE2C, IMR5) (**Fig. 1E-F**). We
134 demonstrate that combining alectinib with indisulam significantly inhibits cell proliferation
135 compared to monotherapies and display great synergy across a wide-range doses of both
136 compounds on neuroblastoma cell lines, but only additive or antagonistic effects were found in
137 KELLY-*DCAF15*$^{KO}$ cell line confirming the necessity of RBM39 degradation for this
138 pharmacological interaction (**Fig. 1E right**). Similar synergy profiles were observed between
139 alectinib and E7820, a second aryl sulfonamide RBM39 degrader (2)(**Fig. S1B-C**).
140
141 In addition, alectinib treatment alone did not induce cell apoptosis, but significantly increased the
142 percentage of apoptotic cells when combined with indisulam in KELLY and IMR32 (**Fig. 2A-B,**
143 **Fig. S2D**). Correspondingly, a significant increase of cleaved caspase 3 was detected in the
144 combination treatment group in KELLY cells (**Fig. 2C**). To evaluate cell cycle progression, we
145 used flow cytometry analysis and detected a notable accumulation of cells in the G2/M phases
146 following 48-hour treatment of indisulam which is consistent with a previous study(16). Co-
147 treatment with indisulam and alectinib increased the percentage of cells in the G1-phase, implying
148 enhanced cell cycle arrest in both G2/M and G1 phase, with a substantial decrease in the percentage

149 of cells in S-phase (**Fig. 2D-E**). These data confirm that indisulam and alectinib act synergistically
150 to suppress the proliferation of neuroblastoma cells, disrupt cell cycle and induce cell apoptosis.
151
152 **ALK inhibition by alectinib is not required for synergistic interaction with indisulam.**
153 According to data from the Human Protein Atlas (proteinatlas.org) (22) ALK and RET, both
154 primary targets of alectinib, are expressed in NB cells but not in HCT116 and KURAMOCHI (**Fig.**
155 **3A, Table S1**) in which synergy was initially discovered. Western blotting confirmed an absence
156 of ALK expression in these cells (**Fig. 3B**). To further test whether the synergy is driven by ALK
157 inhibition, we transfected KELLY, HCT116, and KURAMOCHI cells with an siRNA targeting
158 ALK (siALK) prior to indisulam dosing (**Fig. 3B**). We found no significant difference in cell
159 growth inhibition between siALK and non-targeting control (siNTC) transfected cells (**Fig. 3C**),
160 indicating that ALK inhibition alone does not increase sensitivity to indisulam. We also tested a
161 second ALK inhibitor with a distinct chemical scaffold and binding site, lorlatinib, and found that
162 this compound did not enhance sensitivity to indisulam, except in KELLY cells, which express a
163 mutant, oncogenic form of ALK ($ALK^{F1174L}$) (**Fig. 3D and Fig. S2A**). However, in cell lines with
164 wild type ALK (IMR32) or lacking ALK expression (HCT116 and KURAMOCHI) there was no
165 sensitization (**Fig. 3D**), consistent with other studies (23), indicating that the efficacy of lorlatinib
166 is specific to ALK mutated neuroblastoma. Further experimental validation is needed to clarify the
167 interaction between inhibition of mutant ALK-driven tumours and RBM39 depletion by indisulam.
168 Nonetheless, these findings suggest that ALK inhibition is not a significant contributor to the
169 synergy we observe between alectinib and the RBM39 degraders indisulam and E7820. This
170 suggests that synergy with RBM39 degradation relates primarily to inhibition of a secondary target
171 of alectinib.
172

173 **Alectinib exerts potent inhibition of SRPK1.**

174 Comprehensive kinase inhibitor screens indicate that alectinib inhibits an array of additional
175 kinases other than ALK (19). The observation that alectinib is a potent inhibition of Serine/arginine
176 (SR) Protein Kinase 1/2 (SRPK1/2) (19, 24) is particularly relevant to our research of aberrant
177 RNA splicing. Both SRPK1 and 2 play a central role in regulation of alternative splicing via
178 phosphorylation and activation and nuclear translocation of the Serine/Arginine-rich Splicing
179 Factors (SRSFs) (25, 26). In MYCN-amplified neuroblastoma, SRPK1 expression is elevated and
180 associated with reduced survival rates (**Fig. S2B-C**). In contrast, lower survival rates are not
181 associated with increased expression of SRPK2 nor SRPK3, indicating an increased dependency
182 on SRPK1 to drive tumour growth in MYCN-amplified tumours. Furthermore, a genome-wide
183 CRISPR study showed that loss of SRPK1 sensitizes to indisulam treatment in various solid
184 tumour cell lines (27). Thus, we further explored the treatment combination of SRPK1i and
185 RBM39 degraders. To this end, we assessed the synergy between indisulam and SPHINX31, a
186 known SRPK1 inhibitor(28). Co-treatment of SPHINX31 and indisulam exhibited synergistic
187 growth inhibition cancer across all three cell lines (**Fig. 4A**). Time-lapse cell confluency
188 monitoring in KELLY-*DCAF15*$^{WT}$ and *DCAF15*$^{KO}$ showed that co-treatment significantly
189 suppressed the growth of KELLY-*DCAF15*$^{WT}$, compared to individual drug treatments.
190 Conversely, in the absence of *DCAF15*, the combination therapy displayed similar potency to
191 SPHINX31 monotherapy (**Fig. 4B**), suggesting this interaction is DCAF15-dependent and thus
192 RBM39-dependent.

193

194 The inhibition of SRPK1 by alectinib was confirmed by enzyme activity assays which reported a
195 half-maximal inhibitory concentration (IC50) of 26nM. This inhibition is more potent than that of

196 SPHINX31 (IC50 = 375nM) with lorlatinib showing very little inhibitory action (**Fig. 4C**).
197 Comparison of the crystal structures of the SRPK1-Alectinib and SRPK1-SPHINX31 complexes
198 confirmed that alectinib and SPHINX31 interact with the ATP-binding groove of SRPK1, with
199 reasonable affinity and occupying similar positions within the binding site (**Fig. 4D** and **Fig. S3**).
200 Notably, alectinib inhibited SRPK2 with an IC50 of 700nM while SPHINX31 showed no
201 inhibitory effect (**Fig. S2D**).
202
203 SRPK1 phosphorylates SRSFs, triggering their nuclear translocation and activity in modulating
204 RNA splicing (**Fig. 4E**). Both alectinib and SPHINX31 reduced phosphorylated SRSF (p-SRSF)
205 in KELLY, HCT116 and KURAMOCHI cells (**Fig. 4F)** and decreased the nuclear-to-cytoplasmic
206 ratio of p-SRSF intensity within 4 hours in KELLY cells, while lorlatinib lacked this effect (**Fig.**
207 **4G**). SRSFs are known to promote selection of the proximal splice site in *VEGF* pre-mRNA and
208 inhibiting SRPK1 alters *VEGF* splicing to generate the *VEGF165b* isoform(19, 29). Treatment of
209 both alectinib and SPHINX31 resulted in a switch and increased *VEGF165b* mRNA in high-risk
210 neuroblastoma cells (**Fig. 4H**).
211
212 In conclusion, our findings reveal that alectinib is a potent inhibitor of SRPK1, consequently
213 modulating downstream function and RNA splicing through a reduction in the phosphorylation of
214 SRSF splicing factors. Notably, alectinib demonstrates more robust inhibition of SRPK1 as
215 compared to the selective inhibitor SPHINX31, an intriguing observation that could potentially
216 expedite the clinical repurposing of alectinib as an SRPK1 inhibitor.
217
218

219 **Alectinib and indisulam exacerbate RNA splicing defects, increase R-loop formation and**
220 **DNA damage.**

221 Proteomic data from our previous study (15) showed that indisulam exposure leads to an increase
222 in protein expression of most SRSF family members (**Fig. S4A**). Here, we observed enhanced
223 nuclear translocation of p-SRSF post-indisulam treatment, which was rescued in *DCAF15*$^{KO}$ cells
224 (**Fig. S4B-C**), suggesting that SRPK1/SRSF pathway activation is a compensatory mechanism
225 following RBM39 degradation. RBM39 has previously been identified as a potential SRPK1 target
226 [25] and we observed a direct interaction between RBM39 and SRPK1 in neuroblastoma cells via
227 Proximity Ligation Assay (PLA) (**Fig. S4D**). This supports our hypothesis that the synergy
228 between alectinib and indisulam arises from their combined disruption of RNA splicing, by dually
229 targeting interdependent spliceosomal components, thereby limiting cellular adaptation.

230

231 To evaluate the impact of treatment on alternative splicing, IMR32 cells were treated with
232 alectinib, indisulam, or both for 24 hours. RNA-seq and rMATS analysis revealed that while
233 indisulam induced widespread splicing changes, particularly skipped exons (SE) and that alectinib
234 alone had a milder effect, combination treatment resulted in additional 7,646 altered events (33%)
235 and 1,758 mis-spliced genes (25%) beyond an additive effect (**Fig. 5A)**. Notably, alectinib-affected
236 genes largely overlapped with indisulam targets **(Fig. 5B)**, further supporting the likelihood of
237 functional cooperation between RBM39 and SRPK1. Gene ontology (GO) analysis of alternatively
238 spliced genes revealed enrichment in pathways regulating genome stability, including *DNA repair*,
239 *chromatin remodeling* and *DNA damage response* (**Fig. 5C)**. The significantly affected SE events
240 were plotted following combination treatment, as SE represented the predominant type of splicing
241 alteration. (**Fig. 5D)**. Several most affected events were validated through custom PCR primer

242 design of affected exon regions (**Fig. 5E-F)**, confirming that splicing disruption was significantly
243 enhanced when combining RBM39 degraders and SRPK1 inhibition in both KELLY and IMR32
244 cells (**Fig. 5E-F, Fig. S5A**); such an effect was not observed with lorlatinib or siALK (**Fig. S5B-**
245 **D**). These results suggest the synergy observed between alectinib and indisulam may be attributed
246 to the compound reduction of canonical isoform expression and enhanced functional loss in
247 effected pathways, such as DNA damage repair. For example, expression of the canonical CHK1
248 isoform was nearly abolished by the co-treatment of indisulam with either alectinib or SPHINX31.
249 Moreover, CHK1 protein was depleted following indisulam and alectinib combination treatment
250 (**Fig. S5E**),
251
252 To determine whether splicing-induced depletion of DDR genes increased DNA damage, we
253 assessed γH2AX levels as a marker for DNA double stranded breaks(30). Immunofluorescence
254 and western blot showed significant γH2AX accumulation following combination treatment
255 compared to monotherapies (**Fig. 6A–B, Fig. S6A**). Importantly, this increase was absent when
256 indisulam was combined with lorlatinib (**Fig. S6B–C**), indicating that the effect stems from RNA
257 splicing disruption rather than ALK inhibition.
258
259 R-loops are DNA:RNA hybrids that are a product of intermediate transcription and must be
260 resolved to permit progression of replication forks (31, 32). R-loop accumulation results in
261 transcription-replication collisions, which generate replication stress and double-strand breaks
262 (33). Many R-loop regulatory genes were mis-spliced after combination treatment. For example,
263 BRCA1 interacts with the putative RNA helicase Senataxin (SETX), forming a complex that
264 localizes to R-loops(34) and Fanconi Anemia genes recruit RNA processing enzymes to resolve

265 R-loops generated by moderate replication stress(35), while RIF1 facilitates replication fork
266 protection and efficient restart to maintain genome stability(36). Notably, SR proteins regulated
267 by SRPK1 can also impede R-loop formation(31). Dysregulation of these functions lead to
268 accumulation of unresolved R-loops, replication fork breakage, and genome instability (31).
269
270 We quantitated R-loops using S9.6 antibody(37). Treatment with either alectinib or SPHINX31
271 led to increased nuclear S9.6 staining indicating the accumulation of R-loops. The combination
272 treatment significantly increased R-loop formation as compared to monotherapies (**Fig. 6C-D, Fig.**
273 **S6D-F**). To evaluate replication stress induced by Rloop accumulation(31, 38), we quantified the
274 intensity of phosphorylated RPA32 serine 33 (pRPA), a marker of single-stranded DNA (ssDNA)
275 at stalled replication forks. We observed an increase following exposure to the combination
276 treatment relative as compared to monotherapy (**Fig. 6E, Fig. S6E**). DNA fibre analysis using
277 BrdU and IdU labelling further revealed a reduction in track length and the significantly decreased
278 IdU/BrdU ratio following combination treatment, indicating increased fork stalling and replication
279 stress. Collectively, these findings suggest that dual targeting of SRPK1 and RBM39 leads to the
280 accumulation of unresolved R-loops, promoting replication stress, and contributing to subsequent
281 DNA damage in high-risk neuroblastoma.
282
283 **Combination of indisulam and alectinib improves survival in a Th-MYCN/ALK$^{F1174L}$**
284 **neuroblastoma model**
285 Gain-of-function mutations in ALK account for 10-15% of high-risk neuroblastoma (6). ALK
286 inhibitors have been shown to be safe and effective in treating ALK-driven neuroblastoma in a
287 Phase I trial(39, 40), and are currently being investigated in several Phase III trials(39, 41, 42),

288 highlighting their potential for clinical use in ALK-positive neuroblastoma. Considering the clinic
289 relevance and benefit, we used an allograft mouse model implanted with Th-MYCN/ALK$^{F1174L}$
290 tumour cells derived from genetically engineered mouse models (GEMMs) (**Fig. 7A**).
291

292 Tumour-bearing mice were treated (indisulam 10mg/kg, alectinib 40mg/kg or combination) for 2-
293 weeks with a 45-day follow-up. Both monotherapies significantly enhanced survival however all
294 alectinib treated mice relapsed on treatment and 5/8 mice in the indisulam monotherapy group
295 relapsed after withdrawal of treatment. Complete tumour regression without subsequent relapses
296 resulting in a 100% survival rate were reported in the combination group (**Fig. 7B-C**) consistent
297 with the increased efficacy in-vitro.
298 Tumour samples were collected for pharmacodynamic analysis after 3 days of treatment. Western
299 blotting showed a clear depletion of RBM39 following indisulam and combination therapy,
300 confirming the on-target effect of indisulam (**Fig. 7D**). Furthermore, treatment with 10 mg/kg
301 indisulam reduced MYCN expression, as previously reported by Singh et al (43), suggesting a
302 potential link between RBM39 inhibition and suppression of MYCN (**Fig. 7D**). Additionally, a
303 decrease in p-ALK **(Fig. S7A)**, and a reduction in p-SRSF (**Fig. 7F**) confirmed the on-target effects
304 of alectinib on SRPK1 and ALK. Double strand breaks measured by accumulation of γH2AX foci,
305 were increased in combination therapies (**Fig. 7G**), in line with our observations *in-vitro.* However,
306 indisulam alone did not significantly induce γH2AX accumulation, possibly due to the transient
307 nature of γH2AX focus formation during the DNA damage response. However, clear nuclear
308 fragmentation was observed in mice treated with indisulam and combination therapy (**Fig. 7G**).
309 Importantly, no significant weight loss was observed during the trial, indicating no significant

310 toxicity (**Fig. S7B)**, and we observed no significant RBM39 loss in other organs after 3-day
311 treatment (**Fig. S7C**).
312 Taken together, these data confirm that in neuroblastoma the therapeutic benefit of RBM39-
313 depleting agents can be enhanced through combination with SRPK1 inhibitors, such as alectinib.
314 This study provides proof-of concept for the co-targeting of functionally interdependent splicing
315 factors using repurposed clinical agents to more effectively target aggressive childhood cancers
316 such as neuroblastoma. The strategy could apply more widely to other oncogene-driven cancers
317 that exhibit a high dependency on faithful splicing of mRNA.
318

319 **DISCUSSION**

320 Indisulam has been recently identified as a molecular glue capable of regulating RNA alternative
321 splicing(2). By inducing splicing errors of genes in key oncogenic pathways, indisulam and other
322 spliceosomal inhibitors may render cancer cells susceptible to additional disruptions caused by
323 other anticancer drugs. Thus, it holds potential for implementation as combination therapy. We
324 performed extensive drug screens with FDA-approved anticancer agents which revealed several
325 potential drug-drug interactions with indisulam. Notably, the synergy between indisulam and
326 PARP inhibitors, also observed in our screens, has been corroborated by other studies in high-
327 grade ovarian carcinoma(18, 20), colorectal cancer, and breast cancer(44), giving confidence in
328 our screening approach. Our study also highlights the fact that such screens can reveal beneficial
329 interactions based on polypharmacology(engagement of targets beyond the primary focus of
330 clinical development)(45), presenting novel rationales for drug repurposing.
331

332 High-risk neuroblastoma, which constitutes about 15% of all neuroblastoma cases, is characterized
333 by aggressive behaviour and poor prognosis(7). Gain-of-function mutations in ALK account for
334 10-15% of primary tumours (6), hence a number of trials have investigated the use of alectinib and
335 other ALK inhibitors in this clinical setting. While the more selective ALK inhibitor loratinib has
336 shown greater traction for the treatment of mutant ALK-driven neuroblastoma(39), treatment
337 resistance remains a significant clinical challenge(46). Our study demonstrates that the activity of
338 alectinib against SRPK1 can be exploited therapeutically in combination with other spliceosomal
339 inhibitors. This presents an interesting strategy to treat patients with emerging resistance to ALK
340 inhibitor therapy, including in lung cancer where alectinib has demonstrated much greater clinical
341 use(41) and beyond into other cohorts irrespective of ALK status. While other inhibitors of SRPKs
342 and related SRSF regulators such as Cirtuvivint(47) and TG-003(48) are currently in early
343 development, the fact that an established therapeutic tool can be repurposed in this way could
344 accelerate the clinical testing of SRPK1/2 inhibition and co-targeting of splicing factors as an anti-
345 cancer treatment strategy, particularly in tumours where an ALK inhibitor might normally be
346 indicated.
347
348 While we have successfully demonstrated the principle of co-targeting functionally interdependent
349 splicing as an anticancer strategy, several resulting questions arise. Our investigation into the
350 functional consequences of combined RBM39 degradation and SRPK1 inhibition underscores
351 their interdependency in regulating alternative splicing, but it is not yet clear if RBM39 is a direct
352 target of SPRK1 as has been suggested by global interaction profiling (49) and our co-localisation
353 experiments. More broadly, we need further investigation to understand the interactions and co-
354 regulation of different splicing factors that are also cancer targets such as RBM39 and SPRK1,

355 and to develop more detailed mechanistic models of how these regulate alternative splicing
356 together.
357
358 Interestingly, RNA-seq analysis revealed dual targeting SRPK1 and RBM39 synergiscally
359 amplifies RNA splicing dysfunction and downstream cellular stress. Targeting functionally
360 connected nodes within the splicing machinery may therefore offer an effective strategy to
361 overcome cellular adaptation and enhance therapeutic efficacy in high-risk neuroblastoma.
362 However, as with the targeting of spliceosomal components in general, it is unclear if the sequelae
363 of accumulating R loops, cell cycle arrest, DNA damage and eventual cell death that we observe
364 in combined SRPK1/RBM39 interference are lineage-dependent, driven by the mis-splicing and
365 functional loss of a select set of critical genes, or the cumulative consequence of widespread
366 alternative splicing events across multiple functional pathways. Further work to resolve such
367 mechanistic questions will be important to understand what the most relevant pharmacodynamic
368 readouts will be for future discovery experiments and which predictive biomarkers can best
369 identify patients most likely to benefit from such combinations (i.e. for stratification).
370
371 In summary, the present study elucidates a novel therapeutic approach utilizing the combination
372 of indisulam and alectinib in high-risk neuroblastoma, and our results support a model in which
373 co-treatment indisulam and alectinib synergistically impacts RNA splicing through simultaneous
374 RBM39 degradation and SRPK1 inhibition. This dual RNA splicing interference exacerbates
375 splicing errors in key genes regulating genome stability, leading to R-loop accumulation and
376 increased DNA damage. These events eventually result in cellular apoptosis and growth inhibition
377 in high-risk neuroblastoma *in vitro*, as well as suppression of tumour growth *in vivo*. These insights

shed new light on translating research on spliceosome inhibition into clinical applications, ultimately aiming to improve the prognosis for patients with high-risk neuroblastoma.

## MATERIALS AND METHODS

### Cell lines and cell culture

Human neuroblastoma cell lines were cultured in MEM (Gibco™) with 10% fetal bovine serum (FBS), 1% penicillin/streptomycin (P/S), 1 mM sodium pyruvate, and 2 mM L-glutamine. KURAMOCHI was maintained in DMEM with 10% FBS, 2 mM L-glutamine, 5.6 mM glucose, and 1% P/S. HCT116 was cultured in RPMI 1640 with 10% FBS, 2 mM L-glutamine, and 1% P/S. All cells were authenticated and routinely tested for mycoplasma. Cells were maintained at 37°C with 5% $CO_2$.

### Sulforhodamine B (SRB) assay

Cells were fixed with 10% cold trichloroacetic acid, stained with 0.4% SRB for 30 min, and washed with 1% acetic acid. Bound dye was solubilized in 10 mM Tris-base, and OD measured at 565 nm. Results were normalized to vehicle control.

### Synergy analysis

Cell growth inhibition was assessed by SRB assay after 72 hours of drug exposure. The Loewe additivity model was used to describe the interaction between two agents[32]. Synergy scores were calculated using SynergyFinder web application (RRID:SCR_026127) to compute synergy scores and the Loewe model was selected. Scores >10 indicate synergy, −10 to 10 additivity, and <−10 antagonism.

### Western blotting

400 Whole-cell lysates were prepared using RIPA buffer (Sigma Aldrich) with 1% HALT protease and
401 phosphatase inhibitor cocktail (Thermo Scientific). Equal amounts of protein from each sample
402 were separated on a 4-20% Bis-Tris SurePAGE gel (GenScript) and then transferred onto PVDF
403 membranes. The membranes were blocked with 5% milk for 1 hour at room temperature, followed
404 by an overnight incubation at 4°C with CHK1 (Cell Signaling Technology Cat# 2360,
405 RRID:AB_2080320), p-CHK1 (Cell Signaling Technology Cat# 2348, RRID:AB_331212),
406 γH2AX (Sigma-Aldrich Cat# 05-636, RRID:AB_309864). HRP-conjugated secondaries and
407 chemiluminescent substrate were used for detection.

408 **End-point and quantification PCR reactions**

409 1500ng RNA was utilized for reverse transcription. The resulting cDNA templates were
410 subsequently employed for qPCR using thePowerTrack SYBR Green Master Mix (Applied
411 Biosystems) or End-point PCR utilizing the Q5® High-Fidelity PCR Kit (New England Biolab).
412 PCR products were resolved on 2% agarose gels and quantified with Fiji V2.0.0.

| Target genes | Primer (5' to 3') | Tm |
|---|---|---|
| *BRCA1* | AACTCTGAGGACAAAGCAGC<br>CTTCTCAGTGGTGTTCAAATC | 62 |
| *CHK1* | GTGGAAGACTGGGACTTGGT<br>ACCCCTGCCATGAGTTGATG | 68 |
| *FANCD2* | CGGTTACAGGCTTCCCAAGT<br>GCTGTTCTTGAATGCAGCCT | 67 |
| *FANCI* | GAGTCAGGCCGAGAAGGTTC<br>CAACGGCAGCAGGTTTCTC | 68 |
| *RAD51D* | TGGCTCAGTTCTCGGCTTT<br>AGATGTCAAATGCATGCACCA | 66 |
| *TP53BP1* | GCTGTTGCTGAGTCTGTTGC | 68 |

| | | |
|---|---|---|
| | TGCGTACTTCCCGGATTGTT | |
| *RIF1* | AGGTGGGCAAAACTGGTCAT<br>TGGGTGCTCCACTACGAAAT | 67 |
| *VEGF165b* | AAGAAAATCCCTGTGGGCCTT<br>TGGTGAGAGATCTGCAAGTACGTT | 60 |
| *VEGF165* | AGAGCAAGACAAGAAAATCC<br>TACAAACAAATGCTTTCTCC | 53 |
| *GAPDH* | GGCTGCTTTTAACTCTGG<br>GGAGGGATCTCGCTCC | 62 |

413 **Immunofluorescence staining**

414 KELLY cells were fixed with 4% PFA, permeabilized with 0.1% Triton-X100, and blocked in 5%
415 BSA. Subsequently, they were incubated overnight at 4°C with anti-phosphoepitope SR proteins
416 antibody (1:100, Millipore Cat# MABE50, RRID:AB_10807429) or γH2AX (1:500, Sigma-
417 Aldrich Cat# 05-636, RRID:AB_309864) in blocking buffer ,and then stained with a mix of Alexa
418 Fluor 488-conjugated goat anti-mouse antibody (1:500, AF488, Thermo Scientific), DAPI
419 (1µg/ml, Biotium, Cat#40043), and Phalloidin-647 (1:50, Cell Signaling Technology Cat#
420 #8940S) for 1 hour at room temperature. The cells were washed again three times with PBS-T
421 before imaging with an INCell Analyzer 1000 microscope (GE Healthcare) at 20x magnification.

422 S9.6 (1:250, Millipore Cat# MABE1095, RRID:AB_2861387) and phospho RPA32-S33 (1:250,
423 Novus Cat# NB100-544, RRID:AB_10002227) were detected in KELLY cells fixed with cold
424 methanol at -20°C for 10 minutes and slides were imaged using the Aurox laser-free confocal
425 microscope. To confirm the specificity of the S9.6 antibody, RNase H (Ribonuclease H, 1:100,
426 NEB Cat#M0297S) was applied to the fixed cells before antibody incubation.

427 Image analysis was performed using Cell Profiler V4.2.6, with nuclear regions masked by DAPI
428 staining and cytoplasmic regions masked by Phalloidin staining, excluding areas overlapping with
429 DAPI.

430 **SRPK1/2 kinase activity assay**

431 The SRPK1 Kinase Enzyme System (#VA7558, Promega) and SRPK2 Kinase Enzyme System
432 (#VA7561, Promega) were utilised with the ADP-Glo™ Kinase Assay (#V6930, Promega),
433 following the manufacturer's protocol. Briefly, 1 µl of inhibitor, diluted in 1X kinase reaction
434 buffer, was added to the wells of a 384-well low-volume plate and combined with 8 ng of SRPK1
435 enzyme. Following this, 2 µl of a substrate/ATP mixture (100 µM ATP, 0.1 µg/µl MBP) was
436 added. The reaction was incubated at room temperature for 1 hour. After incubation, 5 µl of ADP-
437 Glo™ Reagent was added to each well, and the plate was incubated at room temperature for 40
438 minutes. Subsequently, 10 µl of Kinase Detection Reagent was added, and the plate was incubated
439 for an additional 30 minutes. Luminescence was recorded.

440 **Proximity Ligation Assay (PLA)**

441 The Duolink® Proximity Ligation Assay (PLA) was used to detect protein-protein interactions in
442 KELLY cells. Samples were fixed with 4% paraformaldehyde, permeabilised with 0.1% Triton X-
443 100, and blocked with the Duolink® blocking solution. Primary antibodies against RBM39 (1:500,
444 Proteintech Cat# 67420-1-Ig, RRID:AB_2882660) and SRPK1 (1:250, Abcam Cat# ab90527,
445 RRID:AB_2050339) were applied overnight at 4°C. Species-specific PLA probes (Sigma-Aldrich)
446 were added, followed by ligation and rolling-circle amplification according to the manufacturer's
447 instructions.

448 **DNA fibre analysis**

449 Cells were sequentially pulse-labeled with 10 μM BrdU and 200 mM IdU for 30 minutes each.
450 KELLY cells were spotted on SuperFrost slides, air-dried for 5 minutes, and lysed with a buffer
451 (200 mM Tris-HCl, pH 7.5, 50 mM EDTA, 0.5% SDS) to release DNA and fixed in 75%
452 methanol/25% acetic acid, and then treated with 2.5M HCl for 1 hour to denature the DNA. After
453 blocking with 1% BSA in PBS-T for 1 hour. BrdU was detected by anti-BrdU antibody (1:50,
454 Abcam Cat# ab6326, RRID:AB_305426)) followed by AF647-conjugated secondary antibody
455 (1:100, A21247, Invitrogen). IdU was labeled with mouse anti-BrdU antibody (1:50, BD
456 Biosciences Cat# 347580, RRID:AB_10015219) and AF488-conjugated secondary antibody
457 (1:100, Thermo Fisher Scientific Cat# A-11001, RRID:AB_2534069). Slides were mounted and
458 imaged using a laser-free confocal microscope, with DNA track lengths measured in Fiji V2.0
459 (RRID:SCR_002285).

460 **In vivo allograft model of neuroblastoma**

461 Syngeneic tumours derived from TH-MYCN/ALK$^{F1174L}$ genetically engineered mouse models
462 (GEMMs), were implanted into immune competent 129×1/SvJ mice. Group assignment was
463 random and treatment began when the implanted tumours reached a volume of over 200 mm³. The
464 dosing schedule continued for 2 weeks, with daily administration for 5 days followed by 2 days
465 off. Alectinib was dissolved in saline containing 40% PEG300, 10% DMSO, and 5% Tween, and
466 was administered orally at a dose of 10 μL/kg. Indisulam was dissolved in saline with 3.5% DMSO
467 and 6.5% Tween80 and was administered intravenously at a dose of 5 μL/kg. Tumour tissues were
468 excised two hours after the final dose of each compound. Half of the tumour was fixed in 4% PFA,
469 while the other half was snap-frozen for subsequent analysis. Investigators were blind for the
470 analysis of the study.

471 **Immunoassays on tissue samples**

472 Snap frozen tumours were lysed in 5% CHAPS buffer and western blotting was carried out for
473 RBM39 (Proteintech Cat# 67420-1-Ig, RRID:AB_2882660), ERK1/2 (Cell Signaling Technology
474 Cat# 4695, RRID:AB_390779), pERK1/2 (Cell Signaling Technology Cat# 9101,
475 RRID:AB_331646), phosphoepitope SR proteins (Millipore Cat# MABE50,
476 RRID:AB_10807429) and GAPDH (Cell Signaling Technology Cat# 2118, RRID:AB_561053).
477 ALK Meso Scale Discovery® immunoassays were performed as previously described(50)

478 **Immunofluorescence on tissue sections**

479 Tumours sections were deparaffinized and rehydrated using Xylene and a graded series of alcohol.
480 They were then boiled in 1% citric-acid buffer for 20 minutes and allowed to cool to room
481 temperature. The sections were blocked for 1 hour in TBS with 0.01% Triton (TBST) and 5%
482 BSA. Afterwards, γH2AX antibody (Cell Signaling Technology Cat# 9718, RRID:AB_2118009)
483 was applied at a 1:100 dilution overnight at 4°C. Alexa Fluor 568 goat anti-rabbit antibody
484 (1:1000) was incubated at room temperature for 1 hour. Images were captured using a confocal
485 microscope (LSM700, LSM T-PMT) and processed with ZEN2009 software (Black version,
486 Zeiss).

487 **RNA sequencing and alternative splicing analysis**

488 Total RNA was extracted and mRNA enriched using poly-T oligo-attached magnetic beads.
489 Strand-specific libraries were constructed and quantified by Qubit and Bioanalyzer and sequenced
490 on an Illumina NovaSeq 6000 platform using an S4 flow cell with 150 bp paired-end reads
491 (Novogene, Cambridge, UK). Sequencing reads were quality-filtered and clean reads were aligned
492 to the human reference genome (hg38) using HISAT2. Gene-level counts were generated using
493 featureCounts, and differential expression analysis was performed using DESeq2. Resulting p-

494 values were adjusted using the Benjamini-Hochberg method to control the false discovery rate
495 (FDR), with significance defined as adjusted p-value ⩽ 0.05

496 Alternative splicing analysis was conducted using rMATS (v4.3.0), which detects five splice event
497 types: skipped exon (SE), mutually exclusive exon (MXE), alternative 5′ splice site (A5SS),
498 alternative 3′ splice site (A3SS), and retained intron (RI). Differential splicing events were
499 identified based on junction-spanning reads, with significance set at FDR < 0.05.

500 **Statistical Analysis**

501 Statistical analyses were conducted using GraphPad Prism 10. For normally distributed data, a
502 Student's t-test was applied to two-group comparisons; one-way or two-way ANOVA for three or
503 more groups. Specific tests are detailed in figure legends.

504

505 **References**


506 1. Patel AA, Steitz JA. Splicing double: insights from the second spliceosome. Nat Rev Mol Cell Biol.
507 2003;4(12):960-70.
508 2. Han T, Goralski M, Gaskill N, Capota E, Kim J, Ting TC, et al. Anticancer sulfonamides target splicing by
509 inducing RBM39 degradation via recruitment to DCAF15. Science. 2017;356(6336).
510 3. Xu C, Chen X, Zhang X, Zhao D, Dou Z, Xie X, et al. RNA-binding protein 39: a promising therapeutic
511 target for cancer. Cell Death Discov. 2021;7(1):214.
512 4. Uehara T, Minoshima Y, Sagane K, Sugi NH, Mitsuhashi KO, Yamamoto N, et al. Selective degradation of
513 splicing factor CAPERalpha by anticancer sulfonamides. Nat Chem Biol. 2017;13(6):675-80.
514 5. Bojko J, Kollareddy M, Szemes M, Bellamy J, Poon E, Moukachar A, et al. Spliceosomal vulnerability of
515 MYCN-amplified neuroblastoma is contingent on PRMT5-mediated regulation of epitranscriptomic and
516 metabolomic pathways. Cancer Lett. 2024;604:217263.
517 6. Matthay KK, Maris JM, Schleiermacher G, Nakagawara A, Mackall CL, Diller L, et al. Neuroblastoma.
518 Nat Rev Dis Primers. 2016;2:16078.
519 7. Bechmann N, Westermann F, Eisenhofer G. HIF and MYC signaling in adrenal neoplasms of the neural
520 crest: implications for pediatrics. Front Endocrinol (Lausanne). 2023;14:1022192.
521 8. Otte J, Dyberg C, Pepich A, Johnsen JI. MYCN Function in Neuroblastoma Development. Front Oncol.
522 2020;10:624079.
523 9. Chen Y, Takita J, Choi YL, Kato M, Ohira M, Sanada M, et al. Oncogenic mutations of ALK kinase in
524 neuroblastoma. Nature. 2008;455(7215):971-4.
525 10. Shaw AT, Gandhi L, Gadgeel S, Riely GJ, Cetnar J, West H, et al. Alectinib in ALK-positive, crizotinib-
526 resistant, non-small-cell lung cancer: a single-group, multicentre, phase 2 trial. Lancet Oncol. 2016;17(2):234-42.

527 11. Alam MW, Borenas M, Lind DE, Cervantes-Madrid D, Umapathy G, Palmer RH, et al. Alectinib, an
528 Anaplastic Lymphoma Kinase Inhibitor, Abolishes ALK Activity and Growth in ALK-Positive Neuroblastoma
529 Cells. Front Oncol. 2019;9:579.
530 12. Lu J, Guan S, Zhao Y, Yu Y, Woodfield SE, Zhang H, et al. The second-generation ALK inhibitor alectinib
531 effectively induces apoptosis in human neuroblastoma cells and inhibits tumor growth in a TH-MYCN transgenic
532 neuroblastoma mouse model. Cancer Lett. 2017;400:61-8.
533 13. Zafar A, Wang W, Liu G, Wang X, Xian W, McKeon F, et al. Molecular targeting therapies for
534 neuroblastoma: Progress and challenges. Med Res Rev. 2021;41(2):961-1021.
535 14. Houghton PJ, Kurmasheva RT. Challenges and Opportunities for Childhood Cancer Drug Development.
536 Pharmacol Rev. 2019;71(4):671-97.
537 15. Nijhuis A, Sikka A, Yogev O, Herendi L, Balcells C, Ma Y, et al. Indisulam targets RNA splicing and
538 metabolism to serve as a therapeutic strategy for high-risk neuroblastoma. Nat Commun. 2022;13(1):1380.
539 16. Singh S, Quarni W, Goralski M, Wan S, Jin H, Van de Velde LA, et al. Targeting the spliceosome through
540 RBM39 degradation results in exceptional responses in high-risk neuroblastoma models. Sci Adv.
541 2021;7(47):eabj5405.
542 17. Anczukow O, Krainer AR. The spliceosome, a potential Achilles heel of MYC-driven tumors. Genome
543 Med. 2015;7:107.
544 18. Xu Y, Spear S, Ma Y, Lorentzen MP, Gruet M, McKinney F, et al. Pharmacological depletion of RNA
545 splicing factor RBM39 by indisulam synergizes with PARP inhibitors in high-grade serous ovarian carcinoma. Cell
546 Rep. 2023;42(10):113307.
547 19. Hatcher JM, Wu G, Zeng C, Zhu J, Meng F, Patel S, et al. SRPKIN-1: A Covalent SRPK1/2 Inhibitor that
548 Potently Converts VEGF from Pro-angiogenic to Anti-angiogenic Isoform. Cell Chem Biol. 2018;25(4):460-70 e6.
549 20. Xu Y, Spear S, Ma Y, Lorentzen MP, Gruet M, McKinney F, et al. Pharmacological depletion of RNA
550 splicing factor RBM39 by indisulam synergizes with PARP inhibitors in high-grade serous ovarian carcinoma.
551 bioRxiv. 2023:2023.01.18.524417.
552 21. BLISS CI. THE TOXICITY OF POISONS APPLIED JOINTLY1. Annals of Applied Biology.
553 1939;26(3):585-615.
554 22. Uhlen M, Bjorling E, Agaton C, Szigyarto CA, Amini B, Andersen E, et al. A human protein atlas for
555 normal and cancer tissues based on antibody proteomics. Mol Cell Proteomics. 2005;4(12):1920-32.
556 23. Infarinato NR, Park JH, Krytska K, Ryles HT, Sano R, Szigety KM, et al. The ALK/ROS1 Inhibitor PF-
557 06463922 Overcomes Primary Resistance to Crizotinib in ALK-Driven Neuroblastoma. Cancer Discov.
558 2016;6(1):96-107.
559 24. Sakamoto H, Tsukaguchi T, Hiroshima S, Kodama T, Kobayashi T, Fukami TA, et al. CH5424802, a
560 selective ALK inhibitor capable of blocking the resistant gatekeeper mutant. Cancer Cell. 2011;19(5):679-90.
561 25. Tufail M, Wu C. SRPKs: a promising therapeutic target in cancer. Clin Exp Med. 2023.
562 26. Nikas IP, Themistocleous SC, Paschou SA, Tsamis KI, Ryu HS. Serine-Arginine Protein Kinase 1
563 (SRPK1) as a Prognostic Factor and Potential Therapeutic Target in Cancer: Current Evidence and Future
564 Perspectives. Cells. 2019;9(1).
565 27. Pogacar Z, Groot K, Jochems F, Dos Santos Dias M, Mulero-Sanchez A, Morris B, et al. Genetic and
566 compound screens uncover factors modulating cancer cell response to indisulam. Life Sci Alliance. 2022;5(9).
567 28. Batson J, Toop HD, Redondo C, Babaei-Jadidi R, Chaikuad A, Wearmouth SF, et al. Development of
568 Potent, Selective SRPK1 Inhibitors as Potential Topical Therapeutics for Neovascular Eye Disease. ACS Chem
569 Biol. 2017;12(3):825-32.
570 29. Amin EM, Oltean S, Hua J, Gammons MVR, Hamdollah-Zadeh M, Welsh GI, et al. WT1 Mutants Reveal
571 SRPK1 to Be a Downstream Angiogenesis Target by Altering VEGF Splicing. Cancer Cell. 2011;20(6):768-80.
572 30. Burma S, Chen BP, Murphy M, Kurimasa A, Chen DJ. ATM phosphorylates histone H2AX in response to
573 DNA double-strand breaks. J Biol Chem. 2001;276(45):42462-7.
574 31. Santos-Pereira JM, Aguilera A. R loops: new modulators of genome dynamics and function. Nat Rev
575 Genet. 2015;16(10):583-97.
576 32. Hamperl S, Cimprich KA. Conflict Resolution in the Genome: How Transcription and Replication Make It
577 Work. Cell. 2016;167(6):1455-67.
578 33. Sridhara SC, Carvalho S, Grosso AR, Gallego-Paez LM, Carmo-Fonseca M, de Almeida SF. Transcription
579 Dynamics Prevent RNA-Mediated Genomic Instability through SRPK2-Dependent DDX23 Phosphorylation. Cell
580 Rep. 2017;18(2):334-43.
581 34. Hatchi E, Skourti-Stathaki K, Ventz S, Pinello L, Yen A, Kamieniarz-Gdula K, et al. BRCA1 recruitment
582 to transcriptional pause sites is required for R-loop-driven DNA damage repair. Mol Cell. 2015;57(4):636-47.

583 35. Okamoto Y, Abe M, Itaya A, Tomida J, Ishiai M, Takaori-Kondo A, et al. FANCD2 protects genome
584 stability by recruiting RNA processing enzymes to resolve R-loops during mild replication stress. FEBS J.
585 2019;286(1):139-50.
586 36. Mukherjee C, Tripathi V, Manolika EM, Heijink AM, Ricci G, Merzouk S, et al. RIF1 promotes replication
587 fork protection and efficient restart to maintain genome stability. Nat Commun. 2019;10(1):3287.
588 37. Phillips DD, Garboczi DN, Singh K, Hu Z, Leppla SH, Leysath CE. The sub-nanomolar binding of DNA-
589 RNA hybrids by the single-chain Fv fragment of antibody S9.6. J Mol Recognit. 2013;26(8):376-81.
590 38. Promonet A, Padioleau I, Liu Y, Sanz L, Biernacka A, Schmitz AL, et al. Topoisomerase 1 prevents
591 replication stress at R-loop-enriched transcription termination sites. Nat Commun. 2020;11(1):3940.
592 39. Goldsmith KC, Park JR, Kayser K, Malvar J, Chi YY, Groshen SG, et al. Lorlatinib with or without
593 chemotherapy in ALK-driven refractory/relapsed neuroblastoma: phase 1 trial results. Nat Med. 2023;29(5):1092-
594 102.
595 40. Suk Y, Singh SK. Safety and efficacy of lorlatinib against ALK-driven refractory or relapsed
596 neuroblastoma. Cell Rep Med. 2023;4(6):101071.
597 41. Peters S, Camidge DR, Shaw AT, Gadgeel S, Ahn JS, Kim DW, et al. Alectinib versus Crizotinib in
598 Untreated ALK-Positive Non-Small-Cell Lung Cancer. N Engl J Med. 2017;377(9):829-38.
599 42. Solomon BJ, Liu G, Felip E, Mok TSK, Soo RA, Mazieres J, et al. Lorlatinib Versus Crizotinib in Patients
600 With Advanced ALK-Positive Non-Small Cell Lung Cancer: 5-Year Outcomes From the Phase III CROWN Study.
601 J Clin Oncol. 2024;42(29):3400-9.
602 43. Singh S, Quarni W, Goralski M, Wan SB, Jin HJ, Van de Velde LA, et al. Targeting the spliceosome
603 through RBM39 degradation results in exceptional responses in high-risk neuroblastoma models. Science Advances.
604 2021;7(47).
605 44. Kohsaka S, Yagishita S, Shirai Y, Matsuno Y, Ueno T, Kojima S, et al. A molecular glue RBM39-degrader
606 induces synthetic lethality in cancer cells with homologous recombination repair deficiency. NPJ Precis Oncol.
607 2024;8(1):117.
608 45. Kabir A, Muth A. Polypharmacology: The science of multi-targeting molecules. Pharmacol Res.
609 2022;176:106055.
610 46. Tucker ER, Jimenez I, Chen L, Bellini A, Gorrini C, Calton E, et al. Combination Therapies Targeting
611 ALK-aberrant Neuroblastoma in Preclinical Models. Clin Cancer Res. 2023;29(7):1317-31.
612 47. Tam BY, Chiu K, Chung H, Bossard C, Nguyen JD, Creger E, et al. The CLK inhibitor SM08502 induces
613 anti-tumor activity and reduces Wnt pathway gene expression in gastrointestinal cancer models. Cancer Lett.
614 2020;473:186-97.
615 48. Sakuma M, Iida K, Hagiwara M. Deciphering targeting rules of splicing modulator compounds: case of
616 TG003. Bmc Mol Biol. 2015;16.
617 49. Buljan M, Ciuffa R, van Drogen A, Vichalkovski A, Mehnert M, Rosenberger G, et al. Kinase Interaction
618 Network Expands Functional and Disease Roles of Human Kinases. Mol Cell. 2020;79(3):504-20 e9.
619 50. Tucker ER, Tall JR, Danielson LS, Gowan S, Jamin Y, Robinson SP, et al. Immunoassays for the
620 quantification of ALK and phosphorylated ALK support the evaluation of on-target ALK inhibitors in
621 neuroblastoma. Mol Oncol. 2017;11(8):996-1006.
622

623

624 **Figure legends**

625 **Figure 1. Combination drug screens revealed a synergistic growth inhibition of indisulam**
626 **and alectinib.** (**A**) Workflow of combination drug screens in HCT116 and KURAMOCHI using
627 indisulam and 147 FDA-approved anticancer compounds. (**B**) Top 20 hits from drug screens in
628 HCT116 (left) and KURAMOCHI (right). HCT116-*DCAF15*$^{WT}$ or HCT116-*DCAF15*$^{KO}$ were
629 treated with selected hits ± indisulam. Bliss scores were calculated from SRB assay data; >0 (red)
630 indicates synergy. KURAMOCHI cells were treated similarly. n=3.; Top 20 hits are ranked by
631 mean bliss score. n=3 replicates. (**C-F**) Cell lines used for synergy screen (C, D) and indicated
632 HRNB cell lines (E, F) were treated with alectinib combining indisulam for 72 hours and analysed
633 for cell growth by SRB. Synergy scores were calculated by Synergyfinder
634 (https://synergyfinder.fimm.fi/) using the Loewe method.

635 **Figure 2. Indisulam and alectinib induce apoptosis and cell cycle disruption in high-risk**
636 **neuroblastoma.** (**A-B**) Apoptosis analysis via flow cytometry in KELLY cells after 48h treatment
637 with 1.25μM indisulam, 4μM alectinib, or their combination. Cells were labelled by Annexin V
638 and propidium iodide (PI). The significance of difference of total apoptotic cells was calculated by
639 one-way ANOVA. (**C**) Western blot of KELLY cells treated with indicated doses of indisulam and
640 alectinib for 48 hours. (n=3 independent experiments) significance of difference was calculated by
641 one-way ANOVA. (**D-E**) Cell cycle analysis by flow cytometry after 48 h treatment with indisulam,
642 Alectinib, or the combination. Cellular DNA content was labelled with PI, replicating cells were
643 labelled with nucleotide analogues 5-Iodo-2-deoxyuridine (IdU). n=3 independent experiments.
644 Two-way ANOVA were employed to determine the statistical significance among the groups. n.s.
645 not significant, * $p < 0.05$, ** $p<0.01$, *** $p < 0.001$, **** $p < 0.0001$.

646 **Figure 3. ALK inhibition by alectinib is not an essential determinant of indisulam synergy.**
647 (**A**) RNA expression data as normalized transcript per million (nTPM) values of cancer cell lines
648 were obtained from proteinatlas.org. (**B**) Western blot confirming the knock-down of ALK gene
649 expression in cells post transfection with siNTC or siALK. (**C**) Indicated cell lines were transfected
650 with siALK or siNTC for 16 hours, followed by exposure to indisulam for 72 hours. Cell growth
651 was measured by SRB assay. (**D**) Indicated cell lines were treated with lorlatinib and indisulam
652 concentration matrix for 72 hours. Loewe synergy scores are plotted. n=3 replicates.
653 **Figure 4. SRPK1 inhibition is synergistic with indisulam in high-risk neuroblastoma.** (**A**)
654 Indicated cell lines were treated with indisulam and SPHINX31. Loewe synergy scores as
655 indicated. (**B**) KELLY-*DCAF15*$^{WT}$ and *DCAF15*$^{KO}$ cells were treated with indisulam and
656 SPHINX31 individually or in combination for 72 hours. Cell confluence was monitored every 6
657 hours using the Incucyte live cell imaging system. One-way ANOVA was used to determine
658 significance. (**C**) SRPK1 enzyme activity measured with ADP-Glo™ Kinase Assay with indicated
659 doses of compounds. (**D**) Alectinib (pink) docked into SRPK1 complexed with
660 SPHINX31(orange). (**E**) Diagram depicting Alectinib inhibition against SRPK1. Made with
661 Biorender. (**F**) Western blotting of p-SRSF in KELLY, HCT116 and KURAMOCHI post-treatment.
662 **(G)** Immunofluorescent staining of p-SRSF in KELLY post-treatment. Nuclear intensity and
663 cytoplasmic staining intensity are calculated using DAPI and Phalloidin (F-actin) segmentation.
664 Scale bar = 20µm. (**H**) qRT-PCR of *VEGF165b* and total *VEGF165* in KELLY and IMR32 cells
665 normalised to GAPDH. * $p < 0.05$, ** $p < 0.01$, *** $p < 0.001$. n = 3 independent experiments.
666
667 **Figure 5. Alternative-splicing elicited in IMR32 cells by treatment with alectinib, indisulam**
668 **and the combination. A.** Number of alternative splicing (AS) events (left) and affected genes

669 (right) detected by rMATS, classified into exon skipping (SE), retained introns (RI), mutually
670 exclusive exons (MXE), alternative 5′ splice sites (A5SS), and alternative 3′ splice sites (A3SS).
671 **B.** Venn diagram showing overlap of alternatively spliced genes across treatments. **C.** Gene
672 Ontology (GO) enrichment analysis of AS genes in the combination group; dot size reflects gene
673 count, colour indicates –logFDR. **D.** Volcano plot of significantly altered exon skipping events in
674 the combination-treated group versus control. For genes with multiple AS events, the one with the
675 largest absolute PSI is shown. Events with FDR = 0 (extremely significant, rounded due to
676 numerical limits) were assigned a nominal value of 1e–15 for display. DDR and genome
677 instability–related genes are highlighted in red, and six of these genes were selected for further
678 experimental validation (labelled). **E.** PCR validation of exon skipping events in DDR genes
679 (representative image of n=3). *GAPDH* was included as a control. **F.** Densitometry analysis of
680 alternative splicing products, Two-way ANOVA was used to detect the significance.
681
682 **Figure 6. Combination of indisulam and alectinib induce DNA damage, R-loop accumulation**
683 **and replication stress. A-B.** Immunofluorescence staining of γH2AX in KELLY cells treated with
684 indisulam in combination of alectinib. Representative images of KELLY treated with 4μM
685 alectinib and 1.25μM indisulam are shown. Scale bars = 20μm. Nuclear foci >5 indicates positive
686 cells. n=3 independent experiments. **C.** Representative images for nuclear S9.6 and RPA32 (S33)
687 foci in KELLY cells, n = 3 independent experiments, Scale bars = 2.5μm. **D-E.** Quantification of
688 nuclear S9.6 intensity (D) and pRPA32 (E) intensity in KELLY cells. Cells were treated with 4μM
689 alectinib monotherapy or with 1.25μM indisulam; nuclear signal intensity were measured by
690 merging to DAPI; n>300 cells from 3 independent experiments were quantified. Significance was
691 analysed among the median values.

692 **Figure 7. Combination of indisulam and alectinib suppress neuroblastoma tumour growth.**
693 (**A**) Th-ALK$^{F1174L}$/Th-MYCN GEMM tumour cells were injected into a cohort of mice
694 subcutaneously, intravenous (i.v.) administration of 10 mg/kg of indisulam and oral gavage (p.o.)
695 40 mg/kg of alectinib for 2 weeks with 5 days on and 2 days off. (**B**) Tumour volume measured 3
696 times a week until the humane end-point was reached. Cyan shade indicates the treatment period.
697 n = 8 for each group. (**C**) Survival plot of mice bearing Th-ALK$^{F1174L}$/Th-MYCN allografts treated
698 with vehicle or alectinib or indisulam or combination therapy. (**D**) Western blotting in tumour
699 tissues after administration of vehicle or alectinib or indisulam or combination therapy for 3 days
700 (n = 4 per group). (**E-H**) Immunofluorescence staining was performed on tumour sections, with
701 DAPI used for nuclear staining. Nuclear p-SRSF intensity (E-F) was measured by merging to
702 DAPI. Nuclear γH2AX (G-H) foci >5 indicates positive cells. Scale bar = 20 μm. n.s. not
703 significant, * $p < 0.05$, ** $p<0.01$, *** $p < 0.001$, **** $p < 0.0001$.

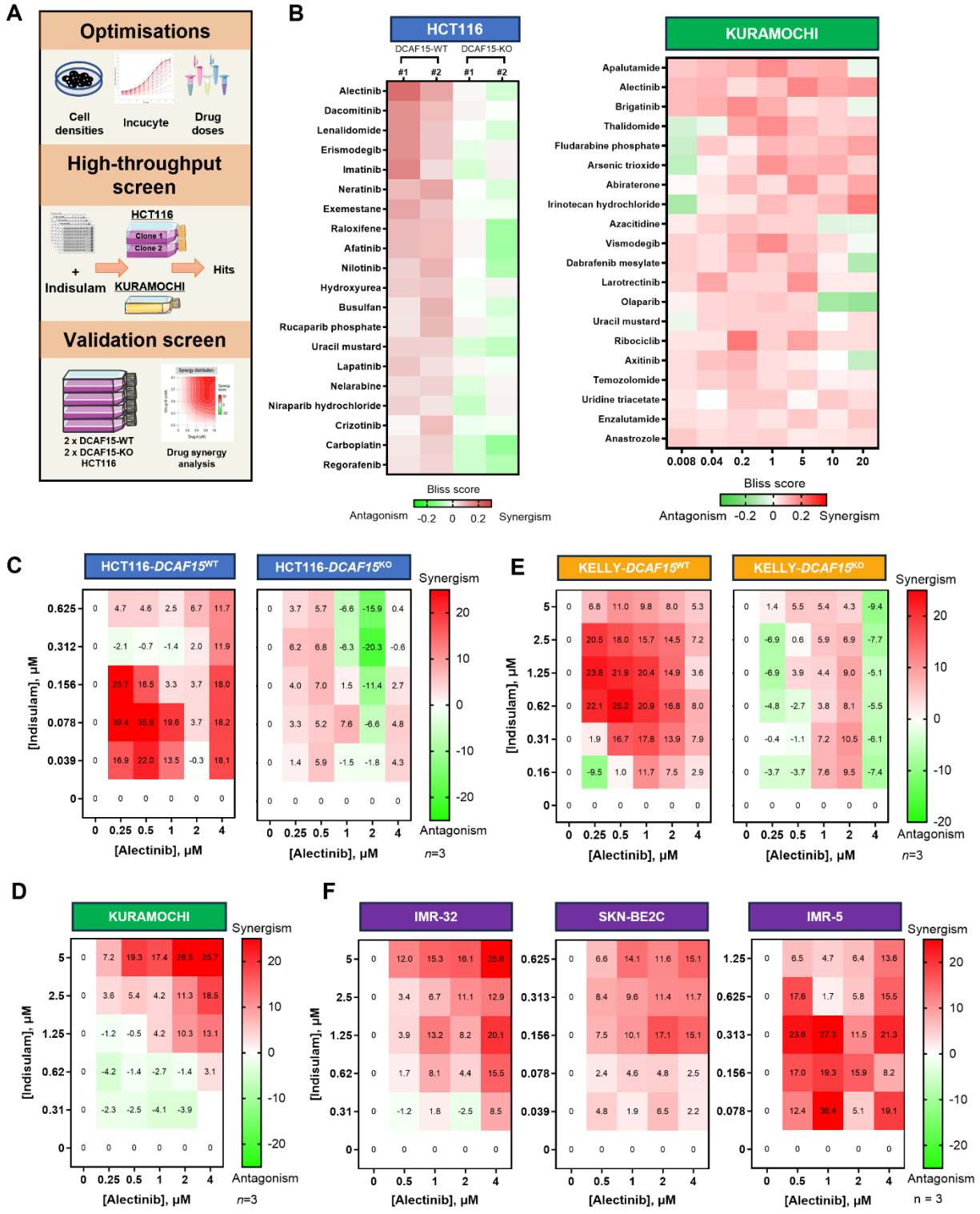
A
Optimisations
Cell densities
Incucyte
Drug doses
High-throughput screen
HCT116
Clone 1
Clone 2
+
Indisulam
KURAMOCHI
Hits
Validation screen
2 x DCAF15-WT
2 x DCAF15-KO
HCT116
Drug synergy analysis
B
HCT116
DCAF15-WT
DCAF15-KO
#1
#2
#1
#2
Alectinib
Dacomitinib
Lenalidomide
Erismodegib
Imatinib
Neratinib
Exemestane
Raloxifene
Afatinib
Nilotinib
Hydroxyurea
Busulfan
Rucaparib phosphate
Uracil mustard
Lapatinib
Nelarabine
Niraparib hydrochloride
Crizotinib
Carboplatin
Regorafenib
Bliss score
Antagonism -0.2 0 0.2 Synergism
KURAMOCHI
Apalutamide
Alectinib
Brigatinib
Thalidomide
Fludarabine phosphate
Arsenic trioxide
Abiraterone
Irinotecan hydrochloride
Azacitidine
Vismodegib
Dabrafenib mesylate
Larotrectinib
Olaparib
Uracil mustard
Ribociclib
Axitinib
Temozolomide
Uridine triacetate
Enzalutamide
Anastrozole
0.008 0.04 0.2 1 5 10 20
Bliss score
Antagonism -0.2 0 0.2 Synergism
C
HCT116-DCAF15WT
HCT116-DCAF15KO
[Indisulam], µM
[Alectinib], µM
Synergism
Antagonism
n=3
E
KELLY-DCAF15WT
KELLY-DCAF15KO
[Indisulam], µM
[Alectinib], µM
Synergism
Antagonism
n=3
D
KURAMOCHI
[Indisulam], µM
[Alectinib], µM
Synergism
Antagonism
n=3
F
IMR-32
SKN-BE2C
IMR-5
[Indisulam], µM
[Alectinib], µM
Synergism
Antagonism
n = 3

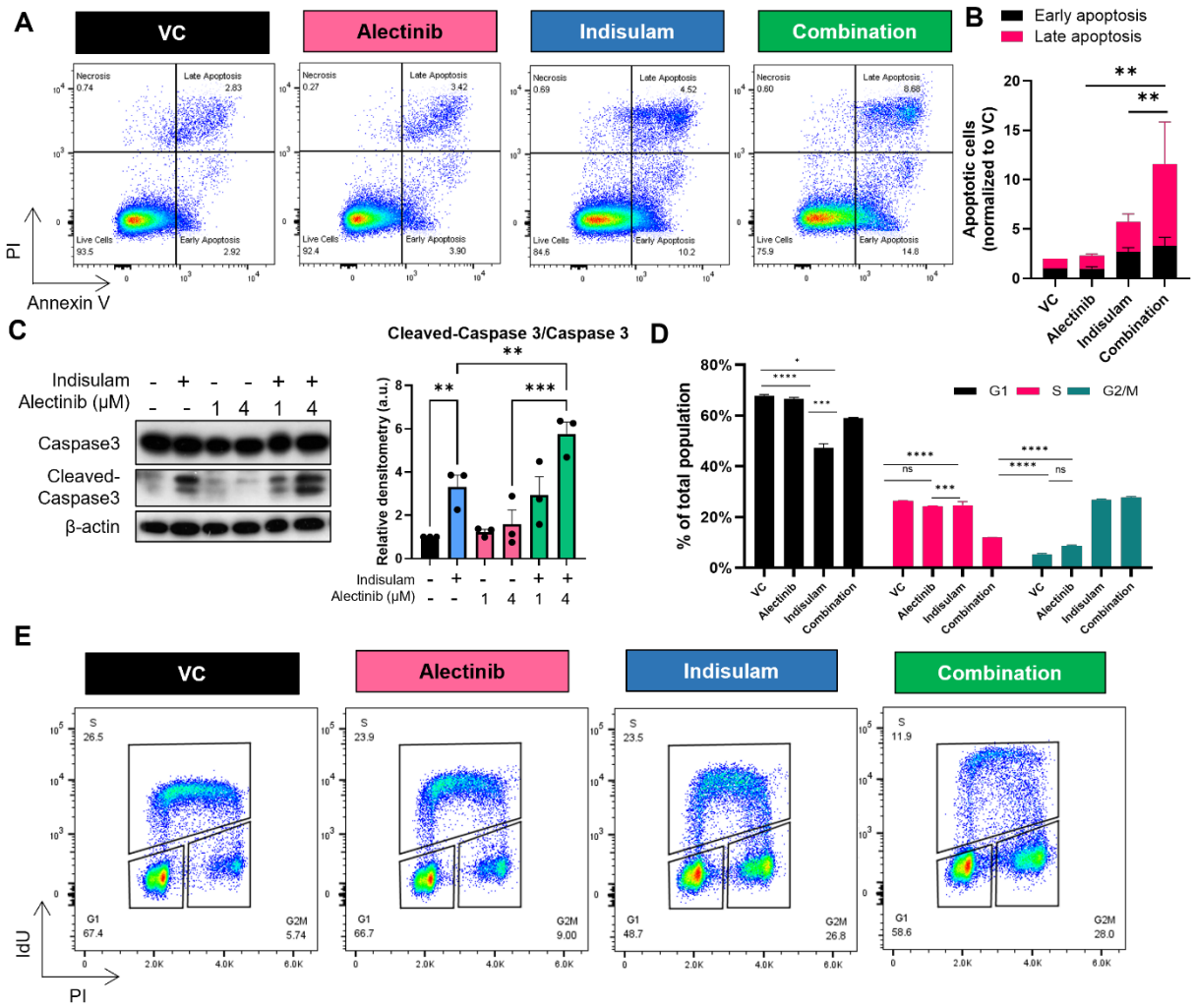
A
VC
Alectinib
Indisulam
Combination
Necrosis
Late Apoptosis
Live Cells
Early Apoptosis
PI
Annexin V
B
Early apoptosis
Late apoptosis
Apoptotic cells (normalized to VC)
C
Indisulam
Alectinib (μM)
Caspase3
Cleaved-Caspase3
β-actin
Cleaved-Caspase 3/Caspase 3
Relative densitometry (a.u.)
D
% of total population
G1
S
G2/M
E
IdU
PI

708 **Figure 3**

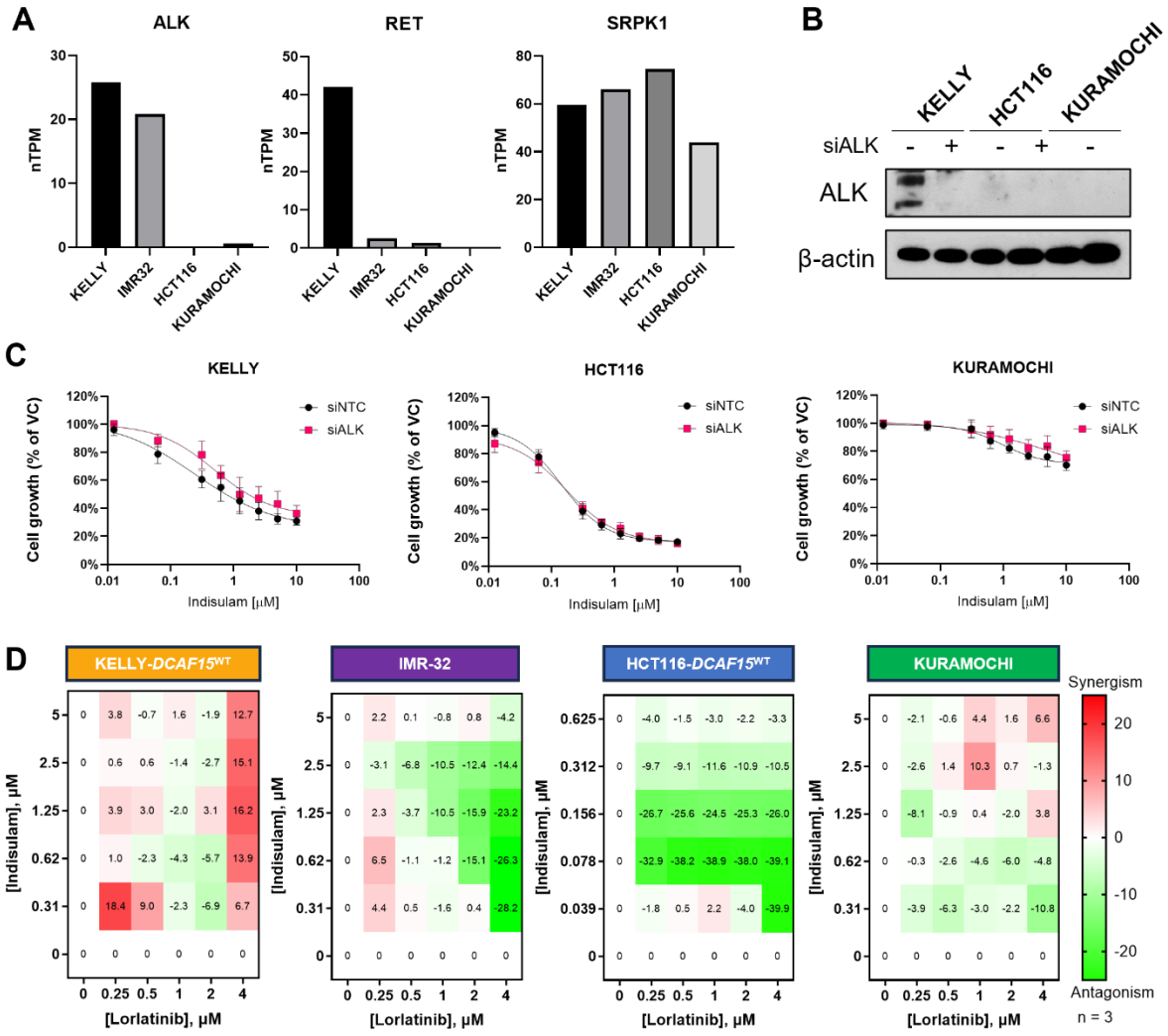


709
710
711

# Figure 4

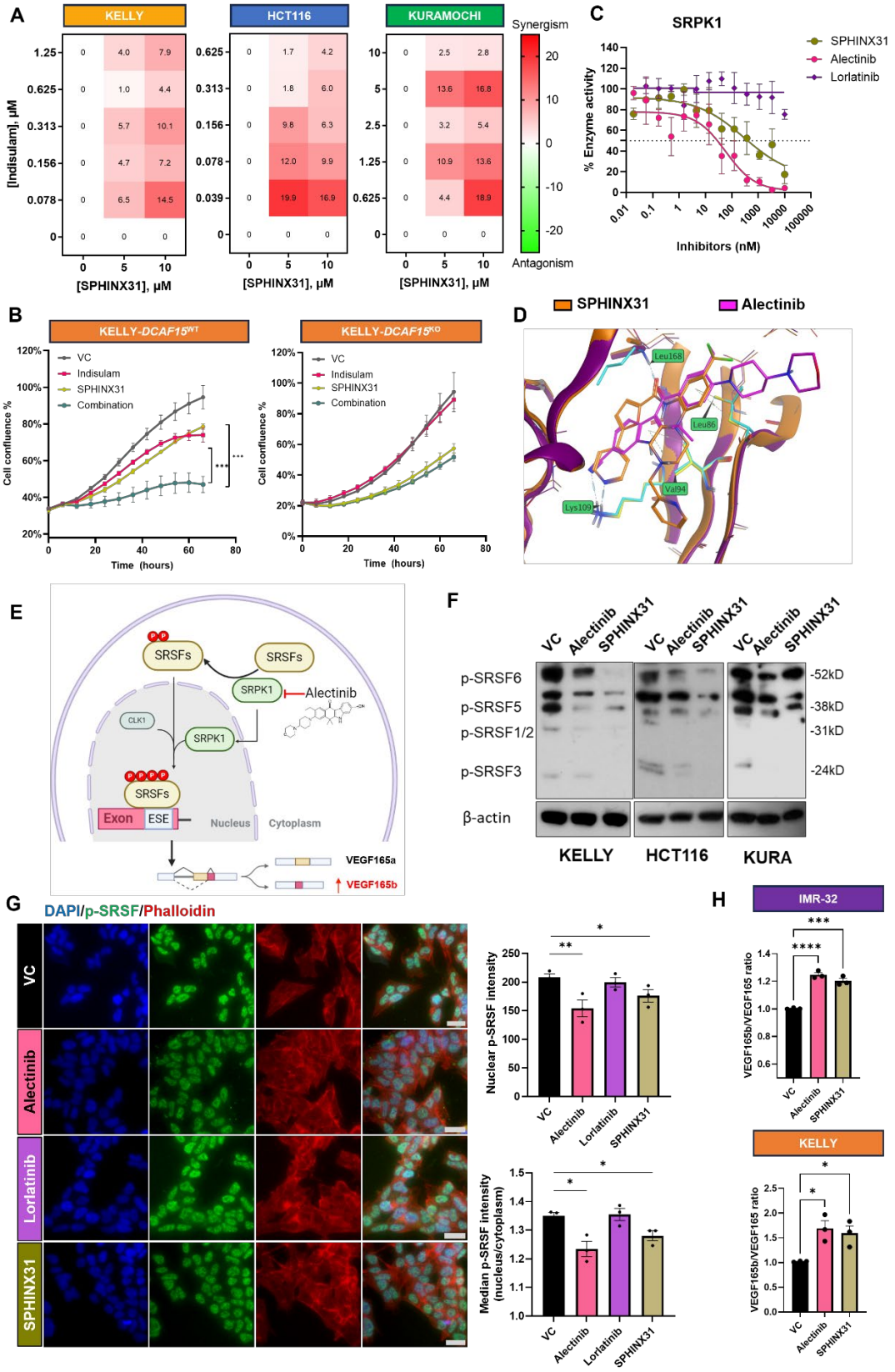
A
KELLY
HCT116
KURAMOCHI
[Indisulam], μM
[SPHINX31], μM
Synergism
Antagonism
C
SRPK1
SPHINX31
Alectinib
Lorlatinib
% Enzyme activity
Inhibitors (nM)
B
KELLY-DCAF15WT
KELLY-DCAF15KO
VC
Indisulam
SPHINX31
Combination
Cell confluence %
Time (hours)
D
SPHINX31
Alectinib
Leu168
Leu86
Val94
Lys109
E
SRSFs
SRPK1
Alectinib
CLK1
Exon
ESE
Nucleus
Cytoplasm
VEGF165a
VEGF165b
F
VC
Alectinib
SPHINX31
p-SRSF6
p-SRSF5
p-SRSF1/2
p-SRSF3
β-actin
-52kD
-38kD
-31kD
-24kD
KELLY
HCT116
KURA
G
DAPI/p-SRSF/Phalloidin
VC
Alectinib
Lorlatinib
SPHINX31
Nuclear p-SRSF intensity
Median p-SRSF intensity (nucleus/cytoplasm)
H
IMR-32
KELLY
VEGF165b/VEGF165 ratio

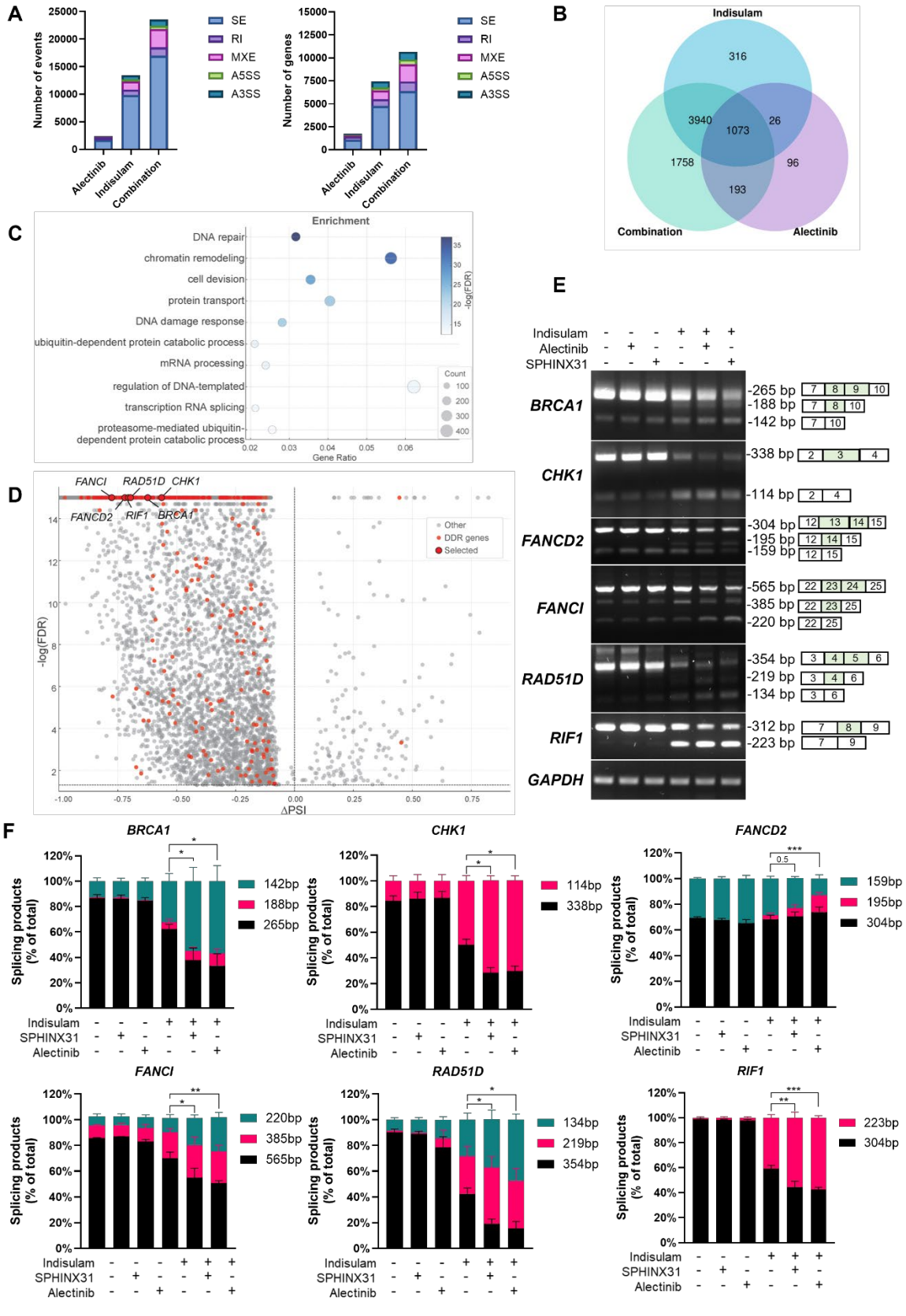
A
Number of events
Number of genes
SE
RI
MXE
A5SS
A3SS
Alectinib
Indisulam
Combination
B
Indisulam
316
3940
1073
26
1758
96
193
Combination
Alectinib
C
Enrichment
DNA repair
chromatin remodeling
cell devision
protein transport
DNA damage response
ubiquitin-dependent protein catabolic process
mRNA processing
regulation of DNA-templated
transcription RNA splicing
proteasome-mediated ubiquitin-dependent protein catabolic process
Gene Ratio
-log(FDR)
Count
D
FANCI
RAD51D
CHK1
FANCD2
RIF1
BRCA1
Other
DDR genes
Selected
-log(FDR)
ΔPSI
E
Indisulam
Alectinib
SPHINX31
BRCA1
-265 bp
-188 bp
-142 bp
CHK1
-338 bp
-114 bp
FANCD2
-304 bp
-195 bp
-159 bp
FANCI
-565 bp
-385 bp
-220 bp
RAD51D
-354 bp
-219 bp
-134 bp
RIF1
-312 bp
-223 bp
GAPDH
F
BRCA1
142bp
188bp
265bp
CHK1
114bp
338bp
FANCD2
159bp
195bp
304bp
FANCI
220bp
385bp
565bp
RAD51D
134bp
219bp
354bp
RIF1
223bp
304bp
Splicing products (% of total)
Indisulam
SPHINX31
Alectinib

716 **Figure 6**

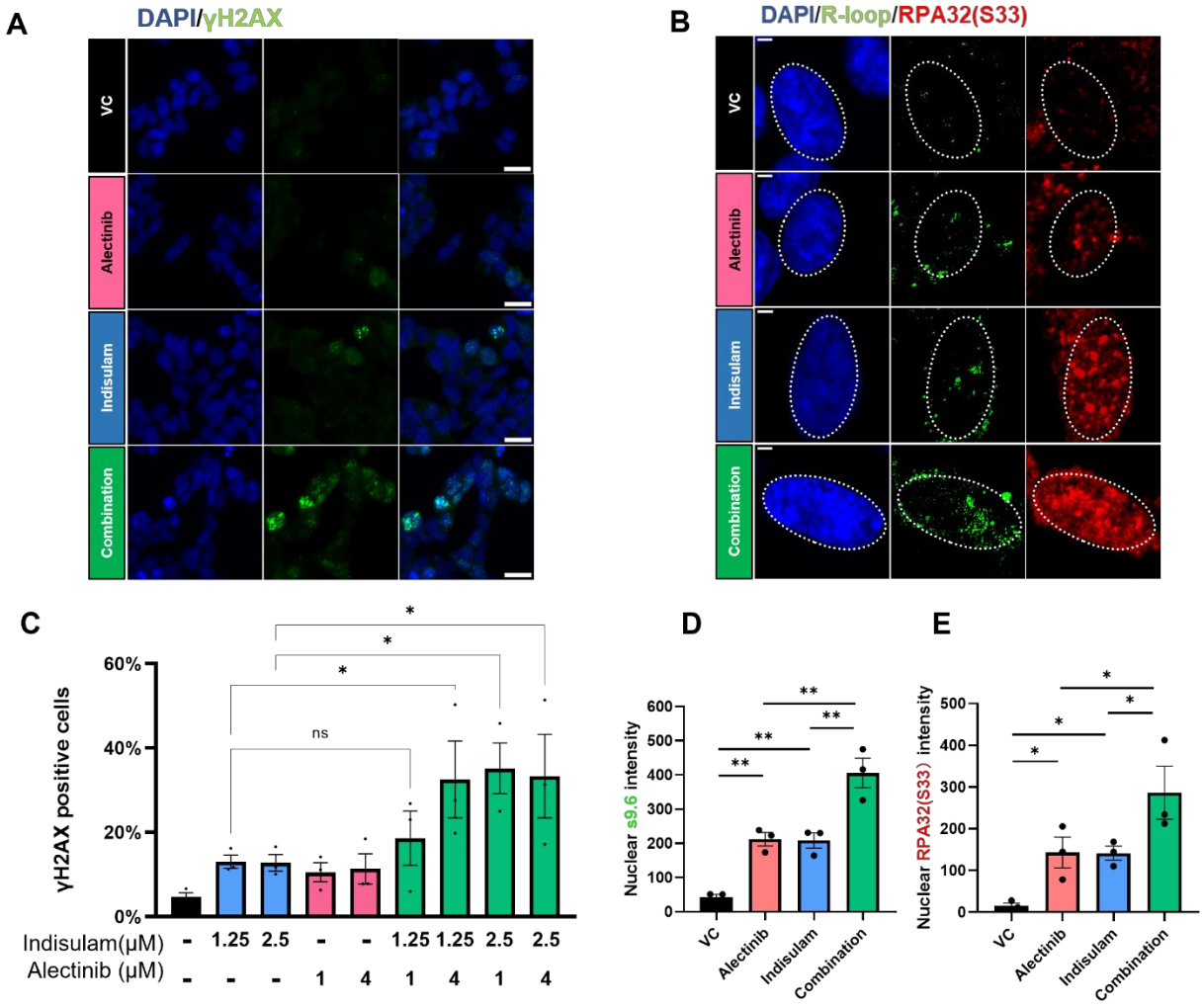


717

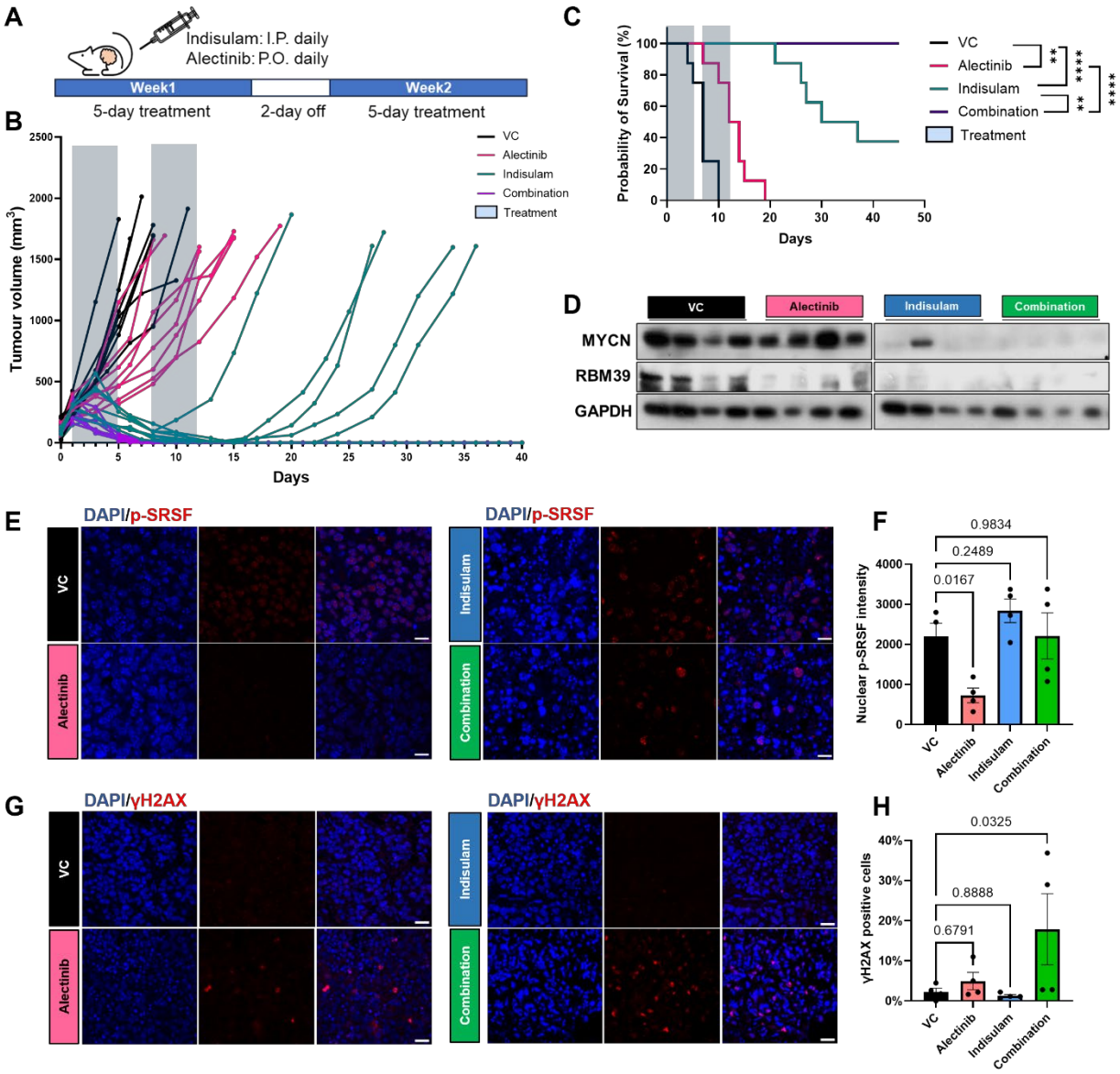
A
Indisulam: I.P. daily
Alectinib: P.O. daily
Week1
Week2
5-day treatment
2-day off
5-day treatment
B
Tumour volume (mm3)
Days
VC
Alectinib
Indisulam
Combination
Treatment
C
Probability of Survival (%)
Days
VC
Alectinib
Indisulam
Combination
Treatment
D
VC
Alectinib
Indisulam
Combination
MYCN
RBM39
GAPDH
E
DAPI/p-SRSF
VC
Alectinib
Indisulam
Combination
F
Nuclear p-SRSF intensity
0.9834
0.2489
0.0167
VC
Alectinib
Indisulam
Combination
G
DAPI/γH2AX
VC
Alectinib
Indisulam
Combination
H
γH2AX positive cells
0.0325
0.8888
0.6791
VC
Alectinib
Indisulam
Combination

720 **Acknowledgments:** We are very grateful to the technicians from the Institute of Cancer
721 Research BSU animal center, Barbara Martins da Costa and Kevin Greenslade for supporting
722 animal work. We thank Prof. Matthew J Fuchter from Imperial College London and Dr Lizzie
723 Tucker from Institute of Cancer Research for providing helpful comments.
724 **Funding:** Imperial College London and China Scholarship Council joint PhD studentship
725 202208310101 (YM), 201808060050 (YX). AstraZeneca/NIHR Imperial BRC Imperial College
726 Research Fellowship (AN). Cancer Research UK Fellowship RCCCDF-Nov23/100003 (AN).
727 Cancer Research UK Discovery Programme Grant (A28278) (EP, BMC, LC); HEFCE/RAE
728 (LC). Ovarian Cancer Action (CW, AN). Cancer Research UK convergence Science Centre PhD
729 studentships SEBCATP-2024/100009 (NZ), CANCTA-2022\100007 (SQ).
730 **Author contributions:**
731 Conceptualization: YM, AN, HCK
732 Methodology: YM, EP, YX, SQ, AN
733 Investigation: YM, EP, BMC, YX, CJ, SQ, NZ, LC, HCK, AN
734 Visualization: YM, YX, CJ, SQ, AN
735 Funding acquisition: LC, HCK, AN
736 Project administration: HCK, AN
737 Supervision: AN, HCK, LC,
738 Writing – original draft: YX, LC, HCK, AN
739 Writing – review & editing: all authors contributed to the review and editing of the paper.
740 **Data and materials availability:** All data supporting the conclusions of this paper are available
741 within the main text and/or Supplementary Materials.
742